Available online at www.sciencedirect.com
ScienceDirect
Biochimica et Biophysica Acta 1768 (2007) 264–279
Biochimica et Biophysica Acta
BBA
www.elsevier.com/locate/bbamem

# Glutamate, water and ion transport through a charged nanosize pore

G. De Luca [a], M.I. Glavinović [b,*]

[a] Department of Chemical Engineering, McGill University, Montreal, PQ, Canada
[b] Department of Physiology, McGill University, 3655 Sir William Osler Promenade, Montreal, PQ, Canada H3G 1Y6

Received 5 June 2006; received in revised form 7 August 2006; accepted 15 August 2006
Available online 30 August 2006

**Abstract**

The transport of transmitter, ions and water through a positively-charged nanopore was investigated through computer simulations. The physics of the problem is described by a coupled set of Poisson–Nernst–Planck and Navier–Stokes equations in a computational domain consisting a cylindrical pore, whose radius ranged from 1 to 8 nm and which was flanked by two compartments representing the vesicular interior and extra-cellular space. The concentration of co-ions is suppressed and of counter-ions enhanced, especially near the pore wall owing to electrostatic interactions. Glutamate (i.e. the transmitter considered) is negatively charged and is simulated as a counter-ion. The electro-kinetically induced pressure due to the movement of ions is negative and very pronounced near the pore wall where the concentration and flux of counter-ions is very high. The water velocity peaks in the pore center, diminishes to zero at the pore wall, but is constant along the pore axis. The mean velocity of the water/fluid is proportional to the vesicular pressure and pore cross-sectional area. Interestingly it is inversely related to the vesicular glutamate concentration. The factors determining the glutamate flux are complex. The diffusive flux generally predominates for narrow pore, and convective flux may dominate for wide pore if the vesicular pressure is high. Surprisingly at low vesicular pressure the mean total glutamate flux per unit cross-sectional pore area is higher for narrow pores. Higher flux is probably due to the rise of glutamate concentration in the nanopore, which is much more pronounced for narrow nanopores, due to the maintenance of approximate neutrality of charges in the pore and on the pore wall. In conclusion intra-vesicular pressure helps 'flushing-out' the transmitter, but the induced pressure 'drags-out' the water into the extra-cellular space.


*Keywords:* Poisson–Nernst–Planck; Navier–Stokes; Fusion pore; Glutamate; Vesicle; Pressure

## 1. Introduction

In the exocytosis of hormones, transmitters or peptides the fusion pore links the vesicular interior with the extracellular fluid and provides a conduit for the secretion of the vesicular content. The interactions between the secreted substances and the wall of the fusion pore are believed to play an important role in regulating the time course of their release. They also may regulate the quantal size [1–6]. However, the mechanisms governing the transport of transmitters through the fusion pore are not well understood. While the flux due to the concentration gradient (diffusion flux) is usually considered [7–9], the flux due to the movement of water caused by the pressure gradient (convective flux), and the flux due to the electrical field generated by the mobile charges (ions, transmitter,...) and fixed charges on the wall of the fusion pore (migratory flux) are often overlooked. The role of the convective flux in transmitter release has been especially controversial. In beige mouse mast cells electrical measurements have shown that the vesicle swells following stimulation [10–12]. Vesicular swelling occurs in beige mouse mast cells [13,14] and in chromaffin cells [15,16] after, and not before membrane fusion. Nevertheless it is accepted that there is an important potentiating role in fusion at the plasma membrane, but also in extrusion of vesicular transmitter content [17–21]. The intra-vesicular swelling pressure has been estimated to be significant ($>10^6$ Pa) [22,23]. Large swelling pressure does not necessitate a large hydrostatic pressure, since substantial water may flow across vesicular membrane with only small hydrostatic gradients, if the aquaporins are present in the vesicular membranes [24]. Nevertheless, the hydrostatic pressure may be large if the vesicular

* Corresponding author. Tel.: +1 514 398 6002; fax: +1 514 398 7452.
*E-mail address:* mladen.glavinovic@mcgill.ca (M.I. Glavinović).

0005-2736/$ - see front matter © 2006 Elsevier B.V. All rights reserved.
doi:10.1016/j.bbamem.2006.08.015

membrane tension associated with vesicular swelling inhibits the water permeability through aquaporin channels, or if the density of aquaporin channels is low [25].

According to recent evanescent wave microscopy studies water is secreted through a widened pore during exocytosis [19], arguing that the intra-vesicular hydrostatic pressure is significant. Several questions however remain to be answered. Assuming that the water viscosity is as in bulk, how large should the intra-vesicular hydrostatic pressure be to produce significant water efflux? The movement of mobile charges will induce additional pressure in the fusion pore. How large is such 'electro-kinetically induced pressure', and how large is the resulting 'electro-kinetically driven flow' of water? How much is the water flux likely to augment the transmitter flux? The charged transmitter molecules will be concentrated around the opposite charges on the wall of the fusion pore, whilst the water flux is the highest in the center of the fusion pore, i.e. there is a spatial mismatch of water flux and ion concentration.

We simulated the fusion pore as a nano-sized cylinder with uniformly positively charged surface connected to two compartments equal in size using the computational methods of continuous nanofluidics [26–32]. The transmitter was glutamate and it was negatively charged. Glutamate concentration in the vesicular compartment varied to evaluate the conditions both in the early and late phase of release. The extra-cellular compartment contained $Na^+Cl^-$ whose concentration did not vary from one simulation to another, but the pressure gradient between two compartments and the surface charge density varied over a wide range. The permeation of ions through ion channels is estimated using the set of Poisson–Nernst–Planck equations [26–28], but we used a coupled system of Poisson–Nernst–Planck and Navier–Stokes equations to calculate the potential, electric field, pressure, fluid and ionic fluxes (diffusive, migratory and convective) in the fusion pore, because the transport of transmitter, water and ions through the fusion pore probably occurs in the presence of significant external pressure. The simulations show that the mean water velocity is approximately proportional to the external pressure and the cross-sectional area of the pore. The pressure induced by the movement of charged particles (ions and transmitter) – 'electro-kinetically induced pressure' – can also be very pronounced and may modulate the water flow driven by the external pressure. The water efflux also modulates the extrusion of transmitter and ions. If the pore is narrow, the diffusion dominates the transmitter efflux, but as the pore widens convective flux becomes more important and can become dominant if the external pressure is high. The flow of water driven by the external pressure or induced by the movement of charged particles can thus be an important factor in 'flushing out the transmitter', but the flux of transmitter molecules and ions driven by the concentration gradient and influenced by the presence of fixed charges, can also be important in 'dragging out the water'.

## 2. Methods

### 2.1. Simulation equations

Poisson–Nernst–Planck (PNP) equations are used to calculate ionic current through a pore for all ionic species. PNP equations are composed of the Poisson (1) and Nernst–Planck (2) equations. The electrostatic potential (Φ) is calculated using Poisson equation

$$-\nabla\varepsilon_0\varepsilon_r\nabla\Phi=\rho \tag{1}$$

where $\varepsilon_0$ is the permittivity of vacuum, $\varepsilon_r$ is the relative dielectric constant of solution. The charge density $\rho$ (mobile and fixed) is given by

$$\rho = F\Sigma z_a c_a (= e\Sigma z_a n_a) \tag{2}$$

where $c_a$ is the molar concentration of ion a [mol/m$^3$], $F$ is a Faraday constant ($9.648\times10^4$ C/mol), $z_a$ is the valence of ion a, $n_a$ is the number density of ion a. The factors influencing the potential in the fusion pore are clear from the above formulation. Potential arises from the fixed charges on the pore wall, the mobile charges inside the pore, and the charges in the solution and on control edges outside the pore. The potential profile in the pore will change if any of the conditions above changes.

The movement (by convection–diffusion–migration) of ionic species in the electrolytic fluid/solution is given by the Nernst–Planck equation

$$J_a = uc_a - D\nabla c_a - m_a z_a F c_a \nabla\Phi \tag{3}$$

where $J_a$ is molar flux [mol/m$^2$ s], $D_a$ and $m_a$ are diffusivity and mobility of ion a ($m_a=D_a/RT$), $u$ is fluid velocity and $F$, $R$ and $T$ are Faraday constant, gas constant [8.315 Jl/(Kmol) and temperature (in Kelvin) respectively. Finally the conservation of ionic mass is given by

$$\nabla\cdot J_a = 0 \tag{4}$$

The electrolytic fluid velocity u that is responsible for the convective transport of ions can be computed from the Navier–Stokes (NS) equations.

$$\rho_f u\cdot\nabla u = -\nabla p + \nabla\cdot\eta(\nabla u + (\nabla u)^T) + F_e \tag{5}$$

describes the conservation of momentum, whilst the conservation of mass is given by:

$$\nabla\cdot u = 0 \tag{6}$$

In these equations $\rho_f$, $\eta$, $p$ are respectively the density, viscosity and pressure of the fluid, while $F_e$ is the electric force per unit volume ($F_e=-\rho\nabla\Phi$).

### 2.2. Geometry, parameters and boundary conditions

In this work we consider a nano-size fusion pore of cylindrical geometry. The computational domain chosen to describe this system is depicted in Fig. 1A. The computational domain represents the fusion pore, a piece of the membrane wall as well as portions of the vesicular interior and extra-cellular spaces. The length of the pore L and of each of the compartments representing the vesicular and extracellular spaces was 10 nm resulting in total length of the computational domain of 30.0 nm. The fusion pore radius $R$ ranged from 1.0 to 8.0 nm, whereas the radius W of the compartments representing the vesicular and extracellular spaces was 11 nm. Symmetry conditions are applied on all variables along the axis of the fusion pore (boundary 4). The boundary conditions for the Nernst–Planck equation are concentrations of $K^+$–glutamate$^-$ and $Na^+$–$Cl^-$ on two external controlling edges of the upper or vesicular compartment (boundaries 1) and lower or extra-cellular compartment (boundaries 2). On the edges of the upper compartment the concentrations of $K^+$–glutamate$^-$ ranged from 5 to 150 mM/l (mol/m$^3$) whilst the concentration of $Na^+$–$Cl^-$ was 0 mM/l. On the edges of the lower compartment the concentration of $K^+$–glutamate$^-$ was 0 mM/l whilst the concentration of $Na^+$–$Cl^-$ was 150 mM/l. Both vesicular and extra-cellular solutions are a simplification of physiological conditions, but necessary ones. We assume that glutamate is negatively charged, with a single negative charge, which remains constant throughout simulations. Moreover glutamate is simply considered as an ion (anion), and the complexities of its shape are ignored. Finally we consider that the positive ion in the vesicle is potassium. Whilst sodium would have been a physiologically more appropriate choice we selected potassium to distinguish it from sodium in the extra-cellular compartment.

At the solution–membrane interface (boundaries 3 and 5) an insulation/symmetry or zero current condition was imposed. The boundary conditions for the Poisson equation were zero potential on both upper and lower controlling

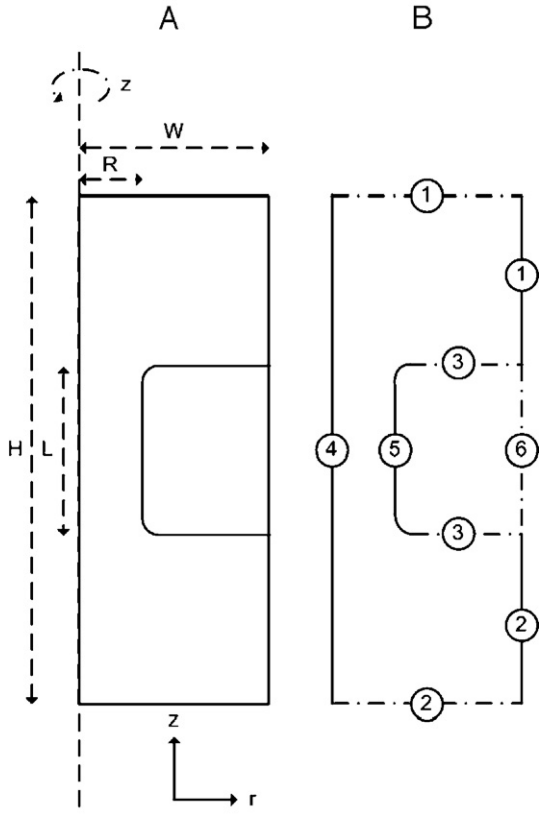


Fig. 1. (A) Semi-schematic of the hemi-section of the computational domain consisting of the cylindrical fusion pore and two compartments—an upper (vesicular) and a lower (extra-cellular) compartment. Three-dimensional model is generated by the rotation of the hemi-section about the central axis by 180°. Fusion pore radius $R$ ranges from 1.0 to 8.0 nm (see Results), whilst the pore length L is 10 nm. The radius W of the compartments representing the vesicular and extracellular spaces is 11 nm. The total length of the computational domain including the fusion pore and two compartments is 30.0 nm. Finally the radii of curvature at the pore entrance and exit are set to 1.0 nm. (B) Boundaries of the computational domain. Boundary conditions are given in Methods.

edges (boundaries 1, and 2). On the internal wall of the fusion pore (including the curved parts on both ends; boundary 5) the surface charge densities ($\sigma$) ranged from $8\times10^{-3}$ to $64\times10^{-3}$ C/m$^2$, which amounts to 3.9 and 30.8 unitary charges respectively for a 1 nm radius nanopore (or 14.3 and 114.6 unitary charges for a 4 nm nanopore). These values are within the range of values estimated for the cell membrane (one elementary negative fixed charge per 1–4 nm$^2$, which corresponds to a charge density of 40–160 C/m$^2$; [33,34]). On the membrane exterior walls (boundary 3) the surface charge density was 0 C/m$^2$. Finally no-slip and no-penetration condition was imposed on the solution–membrane interface (boundaries 3 and 5), or as otherwise specified. The pressure difference between the controlling edges of the upper (boundaries 1) and lower (boundaries 2) compartments varied from $10^4$ Pa to $10^6$ Pa (Navier–Stokes boundary conditions; see Results).

The system of coupled equations given by the PNP and NS equations was solved using the finite element method with adaptive mesh refinement. The mesh independence of the solutions was verified using standard procedures. The diffusion coefficients for ions diffusing freely in bulk aqueous solution are well known [35,36], but it is less clear what they may be in the confined space of the fusion pore, where the interaction electrostatic and non-electrostatic with the walls of the fusion pore [37,38] will restrict ion motion and reduce the diffusion coefficients. We make a simplifying assumption that all diffusion coefficients are spatially uniform, isotropic and the same as in the aqueous solution. Similar assumption is made about the specific viscosity and dielectric constant. The relative dielectric constants of the solution ($\varepsilon_s$) and membrane ($e_m$) were 80 and 2 respectively, but in some simulations the respective values were 40 (nanopore only) and 10. The diffusion constants of $K^+$, $Na^+$, $Cl^-$ and glutamate$^-$ were $1.96\times10^{-9}$, $1.33\times10^{-9}$, $2.03\times10^{-9}$ and $0.76\times10^{-9}$ m$^2$/s, respectively (or were reduced by 80% in the nanopore), the viscosity of the fluid was 1 mPas (or was raised to 2 mPas in the nanopore), whereas the temperature was 300 °K (see Results).

According to the electrical recordings the fusion pores and ion channels are similar [13]. Whilst the ion channels are formed of well-characterized proteins, it is less well known what the structural components of the fusion pore are. Recent studies however suggest that the fusion pore is a lipoprotein structure incorporating soluble *N*-ethylmaleimide-sensitive factor attachment protein receptors (SNAREs) [39,40]. The fusion pore is thus envisioned as a protein (or lipoprotein) consisting of a chain of amino acids folded to form water-filled nanopore controlling the transport of transmitter. The charge on proteins arises from some of the amino acid side chains, the carboxy- and amino-termini, and bound ions. The charge on amino acid side chains depends on the $pK_A$ of the side chains and pH of the solution. When the pH is greater than the $pK_A$ of a group, the deprotonated form predominates, giving acidic side chains a charge approaching −1 and basic side chains a charge approaching 0. In contrast when the pH is less than the $pK_A$ of a group, the protonated form of the group predominates leaving the acidic side chains with a charge approaching 0 and the basic side chains with a charge approaching +1. The charge density on the wall of the fusion pore will thus depend on the pH of the solution in the pore, and may vary depending on the intra-vesicular, but also extra-cellular pH. Vesicular interior is acidified prior to release [41], rendering the fusion pore positively charged, although the charge density will change as pH varies during release as intra-vesicular and extra-cellular solutions come into contact. As the pore dilates, however, the lipid content of the pore increases, and may become a prevailing component of the pore wall, and the negative charge on the phosphatidylserine will alter the charge density on the pore wall previously determined by the protein charges.

### 2.3. Assumptions of continuum modeling of transmitter and ion transport in nanopores

In the derivation of the classical Poisson–Nernst–Planck equation, the ions are assumed to be infinitesimal, the ion–ion, ion–water and ion–wall interactions are all considered in a mean-field fashion (i.e. the molecular aspects of these interactions are neglected). Navier–Stokes equations assume that the fluid density does not vary significantly over intermolecular distances. Several molecular dynamics simulations suggest that the ion distribution near the channel wall are influenced by the discreteness and finite size of the ions and solvent molecules, ion–wall and ion–solvent interactions [31]. However, such contributions though potentially important for very narrow pores are beyond the scope of this paper. The application of PNP theory to ion channels may have additional limitations for channel radii smaller than the Debye length [27], because the dielectric self-energy contribution to the ion's potential energy is not taken into account. This problem can be remedied by the inclusion of an explicit self-energy term in the formalism. Given that in the present study the radius of the fusion pore is typically significantly greater than the Debye length, and given that the inclusion of dielectric self-energy term makes, but only in some cases, the simulations more accurate (in others cases it makes it less accurate) the contribution of the dielectric self-energy was ignored. This is still a developing field of research.

## 3. Results

### 3.1. Spatial distribution of pressure

Fig. 2A, C and E depict the axial profiles (along the z axis in the pore center) of the pressure for a narrow and a wide pore. The pressure in the simulated fluidic system results from the pressure difference between two compartments, but also from the electro-kinetic force near the channel wall (induced pressure). The flow is driven by pressure gradient (external and induced electro-kinetically). Both are largely confined to

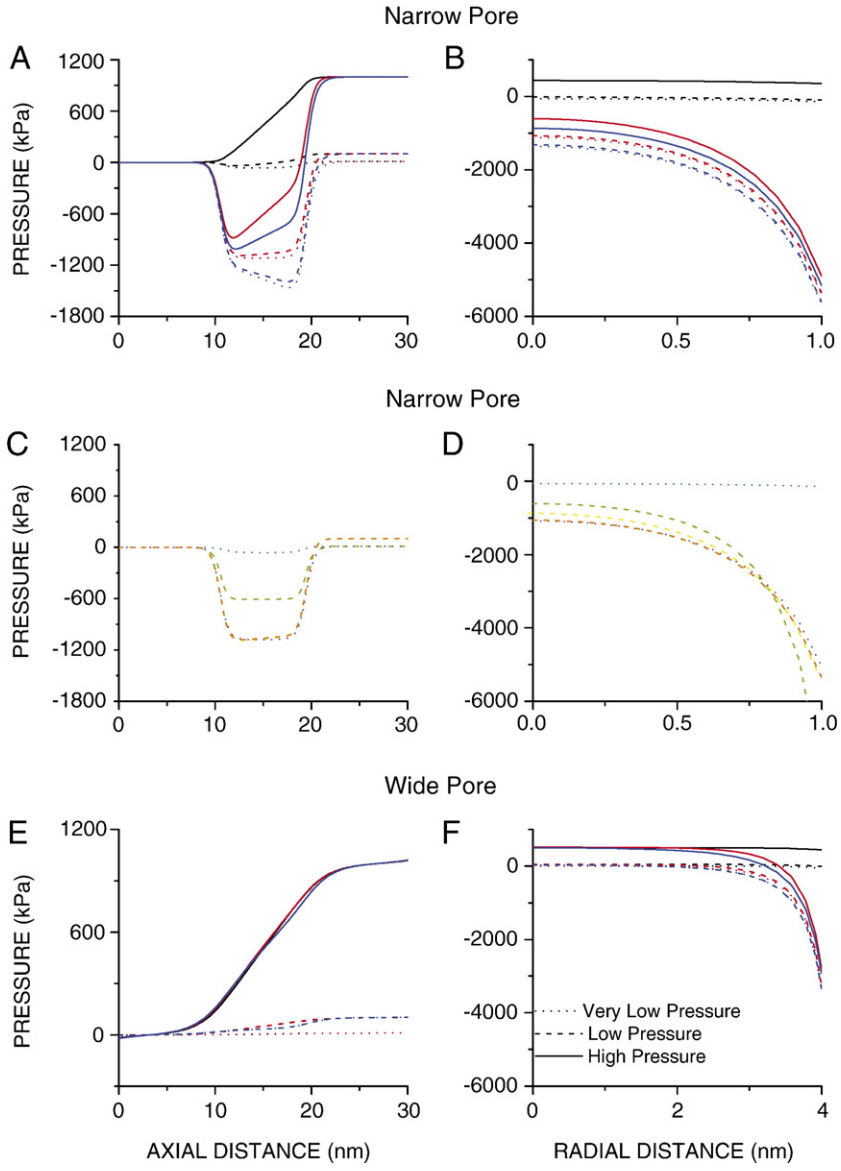


Fig. 2. (A, C and E) The axial pressure profiles. The induced pressure can be very high in the center of the narrow (pore radius of 1 nm), but not wide (pore radius of 4 nm) pore, and may exceed the external and 'maximal' physiological external pressure gradient (see Results). (B, D and F) The radial profile of the pressure in the middle of the pore is essentially uniform if the pore charge density is low, but if the charge density rises a very pronounced (and negative) pressure exists near the pore wall irrespective of the pore radius. Lower nanopore permittivity makes the pressure less negative in the center of nanopore, but more negative near the pore wall. The effects of the lower diffusion constant of ions and glutamate or greater fluid viscosity in the nanopore, or of the greater membrane permittivity are very modest. The pressure difference between the controlling edges of the lower and upper compartments was $10^4$ Pa (very low pressure), $10^5$ Pa (low pressure) and $10^6$ Pa (high pressure). Black, red and blue lines (A, B, E and F) depict the conditions whereby the $K^+$–glutamate$^-$ concentration on the controlling edges of the upper (vesicular) compartment is 150, 150 and 15 mM/l, and the pore wall charge density of 8, 64 and 64 mC/m$^2$ respectively. Other line colors depict following conditions: green (permittivity in the nanopore is 10); dark cyan (slip condition); violet (membrane permittivity—10); yellow (fluid viscosity in the nanopore—2 mPas) and orange (diffusion constants of all ions and glutamate$^-$ in the nanopore reduced by 80%) The pressure on the upper edge was $10^4$ Pa (dark cyan and violet) or $10^5$ Pa (green, yellow and orange). The pore wall charge density was 8 mC/m$^2$ (dark cyan) or 64 mC/m$^2$ (green, violet yellow and orange; B–C) whereas the $K^+$–glutamate$^-$ concentration on the upper edge was 150 mM/l in all cases. $Na^+$–$Cl^-$ concentration on the controlling edges of the upper compartment is 0 mM/l, and on edges of the lower compartment is 150 mM/l (all cases).

the pore interior. The induced pressure becomes more important as the charge density at the pore wall increases, and surpasses the external pressure even though in the example shown the external pressure is near the 'maximal' physiological value of $1.2 \times 10^6$ Pa [22,23]. The induced pressure is negative (leading to a higher total pressure difference in the upper half of the fusion pore), and strongly depends on the pore radius. In the pore center it is very high for a narrow pore, but negligible for a wide pore. Near the wall however, the induced pressure is in both cases very high, and may become several times greater than 'maximal physiological' external pressure difference. The pressure is thus essentially uniform radially irrespective of the pore radius, if the charge density on the pore wall is low, but is highly non-uniform if the charge density is high (Fig. 2B, D

and F). The pressure remains largely the same if the permittivity of the membrane rises from 2 to 10, if the viscosity of the fluid in the nanopore increases from 1 to 2 mPas, if the diffusion constant of ions (and glutamate$^-$) decreases by 80%, or if the no-slip condition changes to slip condition (see Methods; Fig. 2C–D). Lowering the permittivity in the nanopore from 80 to 40 leads however, to a less negative pressure in the pore center, but a more negative pressure near the pore wall (Fig. 2C–D).

### 3.2. Spatial distribution of fluid velocity

Along the z-axis (pore center) the z-component of the fluid velocity is uniform within the pore, irrespective of the external pressure, pore radius or charge on the pore wall (Fig. 3A, C and E). Note that the water efflux is indicated as positive fluid velocity. As expected the external pressure gradient strongly influences the amplitude of fluid velocity, whereas the charge on the pore wall affects it only marginally. Surprisingly the fluid

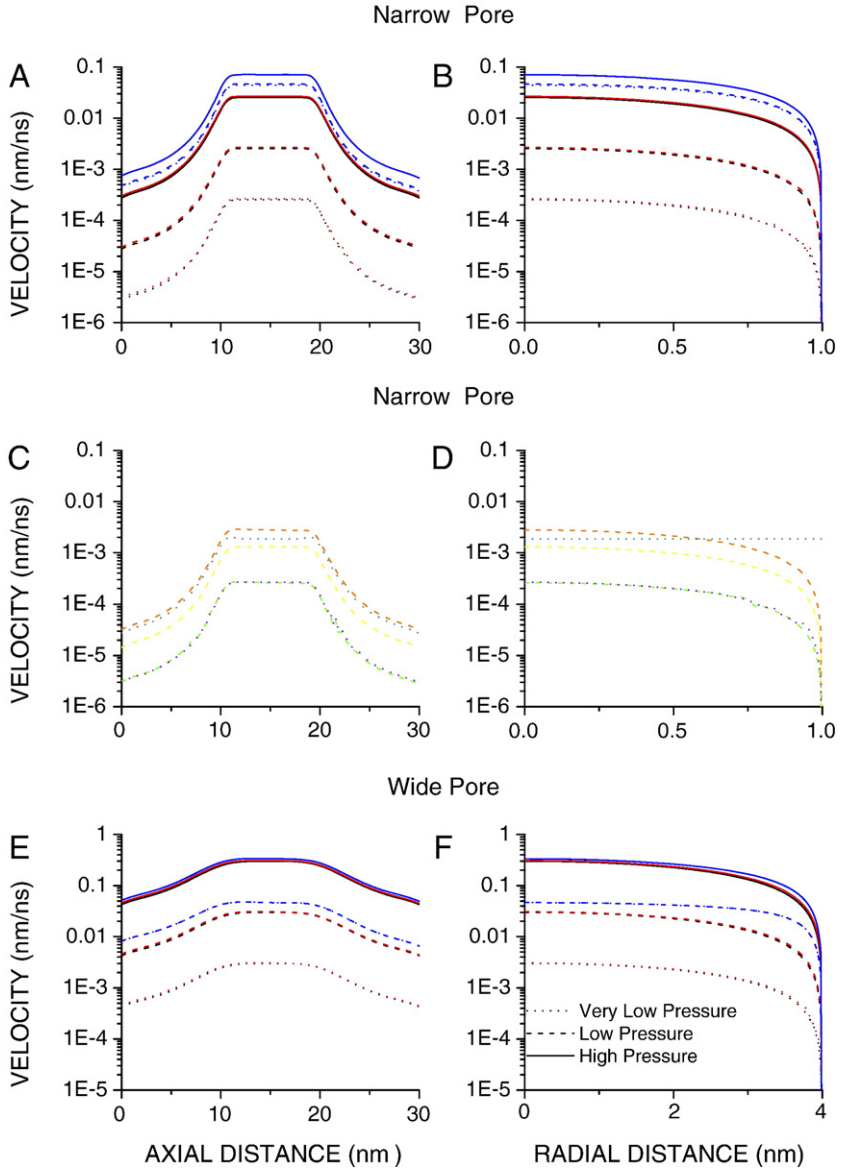


Fig. 3. (A, C and E). The axial profile of fluid velocity (z-component) is uniform within the pore, tapering off rapidly at both ends of the pore, especially if the pore is narrow. The fluid velocity is determined by the external pressure gradient and by the vesicular concentration of $K^+$–glutamate$^-$, increasing as the vesicular glutamate concentration diminishes. (B, D and F) The radial profile of the fluid velocity (z-component) is non-uniform with a maximum in the middle of the pore. Near the pore wall, the velocity diminishes to zero values (no-slip condition; see Methods). The pressure difference between the controlling edges of the lower and upper compartments was $10^4$ Pa (very low pressure), $10^5$ Pa (low pressure) and $10^6$ Pa (high pressure). Black, red and blue lines depict the conditions whereby the $K^+$–glutamate$^-$ concentration on the controlling edges of the upper (vesicular) compartment is 150, 150 and 15 mM/l, and the pore wall charge density of 8, 64 and 64 mC/m$^2$ respectively. Green lines (nanopore permittivity—10); dark cyan (slip condition); violet (membrane permittivity—10); yellow (nanopore fluid viscosity—2 mPas) and orange (diffusion constants of all ions and glutamate$^-$ in the nanopore was reduced by 80%). The pressure on the upper edge was $10^4$ Pa (dark cyan and violet) or $10^5$ Pa (green, yellow and orange; B–C). The pore wall charge density was 8 mC/m$^2$ (dark cyan) or 64 mC/m$^2$ (green, violet, yellow and orange) whereas the $K^+$–glutamate$^-$ concentration on the upper edge was 150 mM/l in all cases. $Na^+$–$Cl^-$ concentration on the controlling edges of the upper compartment is 0 mM/l, and on edges of the lower compartment is 150 mM/l (all cases).

velocity strongly depends on the vesicular concentration of $K^+$–glutamate$^-$, increasing as the vesicular $K^+$–glutamate$^-$ concentration decreases. The fluid velocity tapers off quickly at both ends of the pore, but especially when the pore is narrow. The fluid velocity is the highest in the middle of the pore, whilst at the pore wall it diminishes to zero (Fig. 3B, D and F). Lowering the permittivity in the nanopore (from 80 to 40) or raising it in the membrane (from 2 to 10) has only a marginal effect on the fluid velocity, but the fluid velocity diminishes if the fluid viscosity in the nanopore is raised to 2 mPas from 1 mPas. The greatest increase of the fluid velocity occurs, if the no-slip boundary condition, at the fluid-pore wall interface, changes to slip (see Methods; Fig. 3C–D), which also renders the radial velocity profile flat (Fig. 3D).

### 3.3. Spatial distribution of concentration of charged particles

The axial concentration profiles of $K^+$ and glutamate$^-$ in the pore center differ greatly. The concentration of $K^+$ is low and of glutamate$^-$ high, and the difference depends on the pore width, charge density on the pore wall and vesicular glutamate$^-$ concentration (Fig. 4). The external pressure gradient plays only

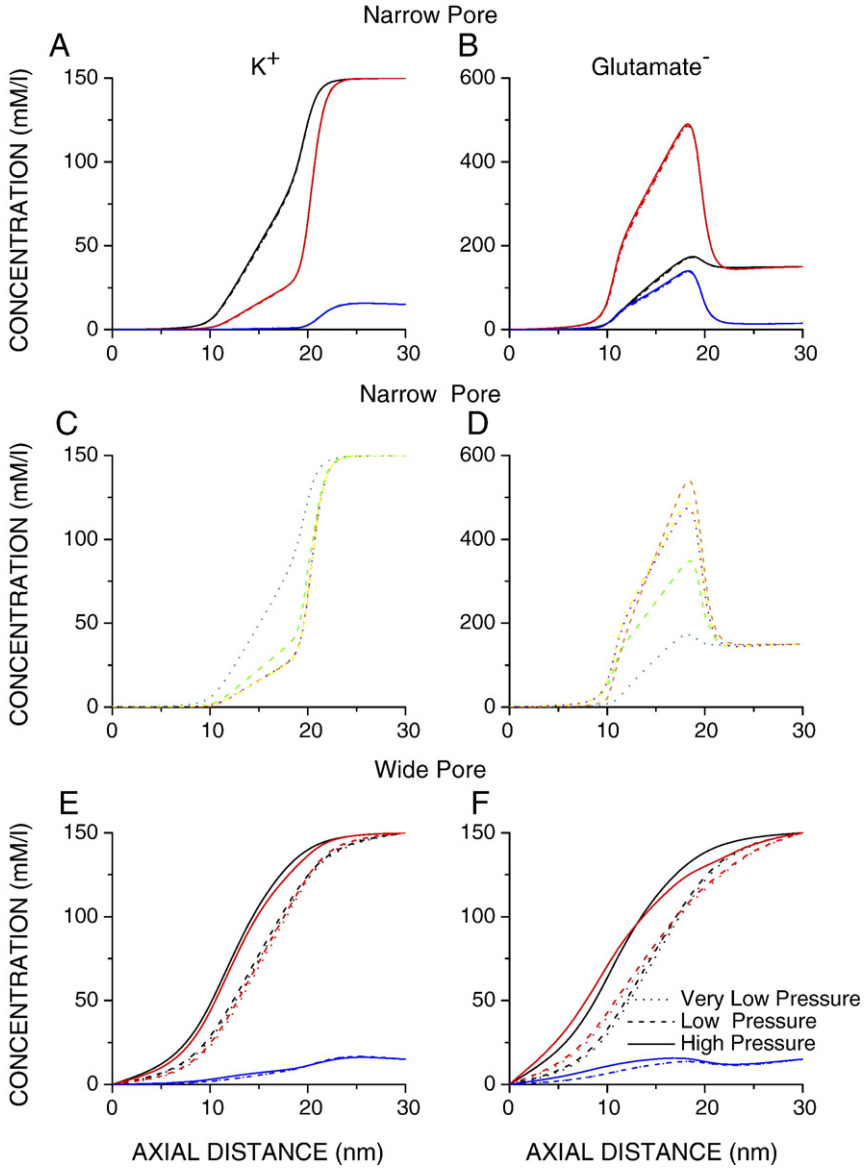


Fig. 4. In the center of narrow pore the axial concentration profiles of $K^+$ and glutamate$^-$ differ greatly, but are similar if the pore is wide. The axial profiles are largely determined by the charge density. The external pressure gradient has only a modest effect, and only if the pore is wide, but enhances the concentration of both $K^+$ and glutamate$^-$. The pressure difference between the controlling edges of the lower and upper compartments was $10^4$ Pa (very low pressure), $10^5$ Pa (low pressure) and $10^6$ Pa (high pressure). Black, red and blue lines depict the conditions whereby the $K^+$–glutamate$^-$ concentration on the controlling edges of the upper (vesicular) compartment is 150, 150 and 15 mM/l, and the pore wall charge density of 8, 64 and 64 mC/m$^2$ respectively. Green lines (nanopore permittivity—10); dark cyan (slip condition); violet (membrane permittivity—10); yellow (nanopore fluid viscosity—2 mPas) and orange (diffusion constants of all ions and glutamate$^-$ in the nanopore was reduced by 80%). The pressure on the upper edge was $10^4$ Pa (dark cyan and violet) or $10^5$ Pa (green, yellow and orange; B–C). The pore wall charge density was 8 mC/m$^2$ (dark cyan) or 64 mC/m$^2$ (green, violet yellow and orange), whereas the $K^+$–glutamate$^-$ concentration on the upper edge was 150 mM/l in all cases. $Na^+$–$Cl^-$ concentration on the controlling edges of the upper compartment is 0 mM/l, and on edges of the lower compartment is 150 mM/l (all cases).

a minor role in shaping the axial concentration profiles when the pore is narrow, but if the pore is wide the concentration of both $K^+$ and glutamate$^-$ rises as the external pressure gradient increases (Fig. 4A–B and E–F). Greater viscosity (yellow line) in the nanopore (2 mPas instead of 1 mPas), or slip boundary condition on the fluid-pore wall interface (instead of non-slip; dark cyan; see Methods) or greater permittivity of the membrane (10 instead of 2; violet) altered the axial concentration profiles of both $K^+$ and glutamate$^-$ only marginally. In contrast, if the nanopore permittivity is reduced to half value (from 80 to 40) the axial profiles of $K^+$ and glutamate$^-$ are clearly altered (green). Reducing the diffusion constant of the ions (and glutamate$^-$) altered the axial profiles also, but only of glutamate$^-$ and only modestly (orange; Fig. 4C–D). Overall the pore wall charge density is the most important factor in suppressing $K^+$ and enhancing glutamate$^-$.

Given large concentration differences in the nanopore depending on the pore size, pore wall charge or external pressure gradient it is interesting to assess how well the nanopore is able to maintain its neutrality. We thus evaluated the ratio of the total charges in the nanopore and the charges on the pore wall. The neutrality of the nanopore was maintained remarkably well and was hardly affected by the external pressure, charge density on the pore wall, vesicular $K^+$–glutamate$^-$ concentration or pore size. For the narrow nanopore (nanopore radius—1 nm) under very low external pressure gradient (pressure gradient—$10^4$ Pa) the ratio was 73.3%, 77.1% and 75.3% with charge on the pore wall and the vesicular $K^+$–glutamate$^-$ concentration being 8 mC/m$^2$ and 150 mM/l, 64 mC/m$^2$ and 150 mM/l and 64 mC/m$^2$ and 15 mM/l respectively. Raising the external pressure gradient to $10^6$ Pa did not lead to any change of the 'neutrality ratio'. The neutrality was better maintained when the pore was wide (radius 4 nm) whereby the corresponding 'neutrality ratios' were higher (80.0%, 81.5% and 79.4%). When the external pressure gradient was raised to $10^6$ Pa, the 'neutrality ratio was affected, but only marginally (<2%).

Radial concentration profiles of $K^+$ and glutamate$^-$ also differ depending on the pore wall charge density (Fig. 5). Near the pore wall their concentrations are largely independent of the pore width, but in the middle of the pore the glutamate$^-$ concentration is greater, and $K^+$ concentration lower for narrow pores, but not for wide pores. The external pressure gradient influences only marginally the $K^+$ or glutamate$^-$ radial distributions of narrow pores, but enhances both if the pore is wide. Finally, note that lower nanopore permittivity, which leads to higher $K^+$ and lower glutamate$^-$ concentration in the pore center reverses its trend and leads to lower $K^+$ and greater glutamate$^-$ concentration near the pore wall (Fig. 5C–D).

### 3.4. Spatial distribution of $K^+$ and glutamate$^-$ fluxes in fusion pore

In a narrow pore the diffusive, migratory and convective $K^+$ fluxes have similar distributions, but the diffusive $K^+$ flux clearly dominates, except when the vesicle is partially empty, when the convective and migratory $K^+$ fluxes make, though a comparatively small contribution (Fig. 6A, C and E). All $K^+$ fluxes are maximal in the pore center, but whilst the diffusive (and migratory) fluxes diminish, the convective fluxes are reduced to zero at the pore wall (a consequence of no-slip condition; see Methods). Diffusive $K^+$ flux also decreases if the charge density on the pore wall, or the vesicular $K^+$–glutamate$^-$ concentration, diminishes.

Diffusive glutamate$^-$ flux also dominates other glutamate$^-$ fluxes, except when the vesicle is partially empty, when the convective (if the external pressure is high) and migratory glutamate$^-$ fluxes make a contribution (Fig. 6B, D and F). Unlike diffusive $K^+$ flux diffusive glutamate$^-$ flux is maximal near the pore wall (the maximal value increases as the charge density on the pore wall rises), whilst the convective glutamate$^-$ flux (and convective $K^+$ flux) decreases to a zero value at the pore wall. Migratory glutamate$^-$ flux can be ignored except for the partially empty vesicle, when it is significant and its direction is into the vesicle. The radial distribution of the total glutamate$^-$ flux depends on the charge density, and on whether the vesicle is full or partially empty.

The changes of the radial profiles of the total $K^+$ and glutamate$^-$ fluxes induced by the changes of the nanopore viscosity, permittivity and diffusion constant of ions (and glutamate$^-$), or the fluid–membrane interface boundary conditions from no-slip to slip are largely, but not entirely, as predicted from the changes of the $K^+$ and glutamate$^-$ concentration (Fig. 7). Changing the nanopore viscosity, or altering the non-slip to slip boundary condition on the fluid membrane interface does not discernibly alter the radial profiles of $K^+$ or glutamate$^-$ fluxes (except for the partially empty vesicles), whereas altering the permittivity in the nanopore changes the radial profiles of $K^+$ and glutamate$^-$ but as predicted from the changes of their concentrations (Fig. 7E–F). However, whereas the reduction of the diffusion constant of ions (and glutamate$^-$) in the nanopore by 80% did not change significantly the concentration profiles of $K^+$ and glutamate$^-$ their flux profiles are clearly different. $K^+$ and glutamate$^-$ fluxes are reduced except for the partially empty vesicle.

Finally note also that the contribution of different fluxes to the total flux will differ depending on the nanopore radius. The most important difference between the total fluxes (of $K^+$ or glutamate$^-$) for the wide and narrow pore is due to the contribution of convective flux, which is much greater and which dominates if the external pressure is high (Fig. 8).

### 3.5. Mean unitary glutamate fluxes

It is clear from the above analysis that the glutamate$^-$ flux through the fusion pore depends on the variety of 'physical' factors (external pressure, concentration gradient, charge density on the pore wall…), and geometric factors (pore radius). To separate the contributions due to the physical factors from those due to geometry, and to be able to compare the fluxes across different geometries we averaged glutamate$^-$ fluxes (total, diffusive, migratory and convective) across the cross-sectional pore area in the pore center. 'Mean unitary' fluxes were calculated using the following equation: $\bar{J}_a = \int J_a \, dS / \int dS$,

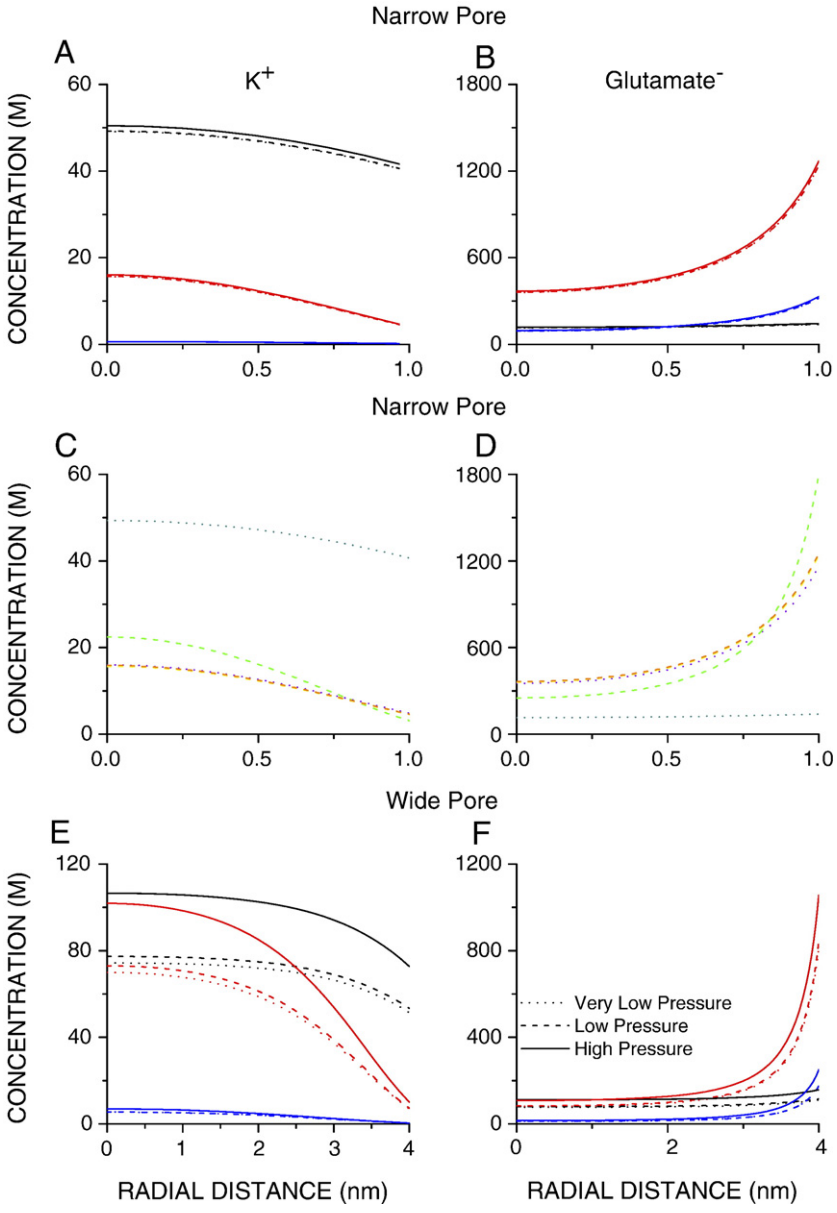


Fig. 5. The radial concentration profiles (middle of the pore) of co-ions ($K^+$) and counter-ions (glutamate$^-$) differ for both narrow and wide pores, and the difference increases as the charge density on the pore wall rises. The concentration of co-ions is reduced and of counter-ions increased and the effect is greater for narrow pores. The external pressure gradient alters the radial concentration profiles only modestly but greater external pressure gradient enhances the concentration of both $K^+$ and glutamate$^-$. The pressure difference between the controlling edges of the lower and upper compartments was $10^4$ Pa (very low pressure), $10^5$ Pa (low pressure) and $10^6$ Pa (high pressure). Black, red and blue lines depict the conditions whereby the $K^+$–glutamate$^-$ concentration on the controlling edges of the upper (vesicular) compartment is 150, 150 and 15 mM/l, and the pore wall charge density of 8, 64 and 64 mC/m$^2$ respectively. Green lines (nanopore permittivity—10); dark cyan (slip condition); violet (membrane permittivity—10); yellow (nanopore fluid viscosity—2 mPas) and orange (diffusion constants of all ions and glutamate$^-$ in the nanopore was reduced by 80%). The pressure on the upper edge was $10^4$ Pa (dark cyan and violet) or $10^5$ Pa (green, yellow and orange; B–C). The pore wall charge density was 8 mC/m$^2$ (dark cyan) or 64 mC/m$^2$ (green, violet yellow and orange) whereas the $K^+$–glutamate$^-$ concentration on the upper edge was 150 mM/l in all cases. $Na^+$–$Cl^-$ concentration on the controlling edges of the upper compartment is 0 mM/l, and on edges of the lower compartment is 150 mM/l (all cases).

where $J_a$ is the glutamate$^-$ flux at any point on a cross-sectional surface area S in the middle of the fusion pore). As already concluded the diffusive glutamate$^-$ fluxes dominate when the pressure gradient is low, except when release occurs from the partially empty vesicles. The simulations that completely ignored the interactions of glutamate$^-$ (but also of $K^+$, $Na^+$ and $Cl^-$) with water (i.e. simulations that used only Poisson–Nernst–Planck equations and ignored Navier–Stokes equations) had very similar total glutamate$^-$ fluxes, except when the nanopore widened significantly (Fig. 9A, C and E). More interestingly the mean unitary diffusion (and total) glutamate$^-$ fluxes are typically higher when the pore is narrow, and the dependence is especially pronounced when the charge density on the pore wall is high (Fig. 9). Note nevertheless that for low charge density pores the mean unitary diffusion (and total) glutamate$^-$ fluxes increase following an initial decrease as the

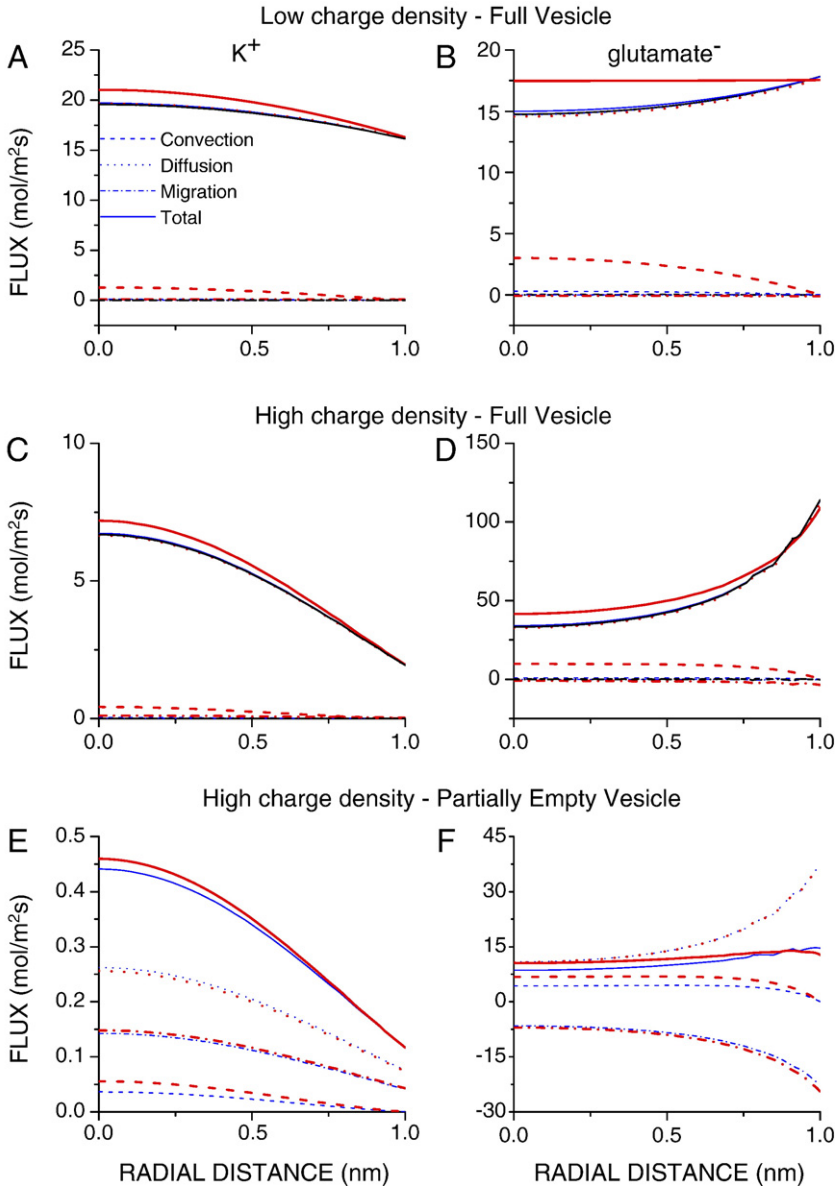


Fig. 6. Vesicular concentration of $K^+$–glutamate$^-$, pore charge density and external pressure gradient all affect the radial distribution of diffusive, migratory and convective fluxes in the middle of the narrow pore (radius of 1 nm). The diffusive fluxes predominate but the convective and migratory fluxes make a significant contribution when the vesicle is partially empty. The fluxes usually diminish near the pore wall and the convective fluxes become zero (see text). The external pressure difference was $10^5$ Pa (blue lines) or $10^6$ Pa (red lines). The charge density on the pore wall was either 8 mC/m$^2$ ('low charge density') or 64 mC/m$^2$ ('high charge density'). $K^+$–glutamate$^-$ concentration on the controlling edges of the upper (vesicular) compartment was 150 ('Full Vesicle') or 15 mM/l ('Partially Empty Vesicle'). $K^+$–glutamate$^-$ concentration on the controlling edges of the lower (extra-cellular) compartment was 0 mM/l in all cases. $Na^+$–$Cl^-$ concentration was 0 mM/l (controlling edges of the upper compartment) and 150 mM/l (controlling edges of the lower compartment) in all cases.

nanopore widens (Fig. 9A). Finally the total fluxes rise significantly when the external pressure gradient rises (especially if the pore is wide) due to the contribution of the convective flux, which completely dominates.

### 3.6. Mean fluid velocity

Fig. 10 shows the dependence of the mean fluid velocity (calculated using the following equation: $\overline{u}=\int u\,dS/\int dS$, where $u$ is the fluid velocity at any point on a cross-sectional surface area $S$ in the middle of the fusion pore) on the charge density of the fusion pore, vesicular glutamate concentration, fusion pore cross-sectional area and the external pressure. We restrict our analysis to nanopores with radii ranging from 1 to 4 nm as they provide clear trends for the relationships examined. The mean fluid velocity rises, but only marginally as pore wall charge density increases (Fig. 10A). More interestingly the mean fluid velocity is generally higher when the vesicular glutamate concentration is lower (partially empty vesicles; Fig. 10B). As expected the mean velocity rises though sub-linearly with the pore cross-sectional area (Fig. 10C), but the dependence of the mean velocity on the external pressure is almost linear (Fig. 10D), and the slope of the mean velocity vs. pressure relationship also rises almost linearly (Fig. 10E).

## 4. Discussion

### *4.1. Simulation of transport through a charged nanofluidic pore*

Ion distributions and velocity profiles for electro-osmotic flow in nanopores of different widths were studied using continuum theory. The potential and concentration profiles in nanopores can be calculated using either Poisson–Boltzmann or Poisson–Nernst–Planck theories [27,42]. Poisson–Boltzmann theory is however, restricted to equilibrium problems, and transport of ions or charged transmitter molecules is a non-equilibrium problem requiring Nernst–Planck electrokinetic equation. Nernst–Planck equation combines Fick's law of diffusion due to a concentration gradient and Ohm's law for drift of ions in a potential gradient. If Poisson's equation is used to calculate the potential in Nernst–Planck equation, such a set of equations forms the Poisson–Nernst–Planck theory, which provides a powerful and widely used theoretical tool for simulation of many problems in physics and chemistry [43,44].

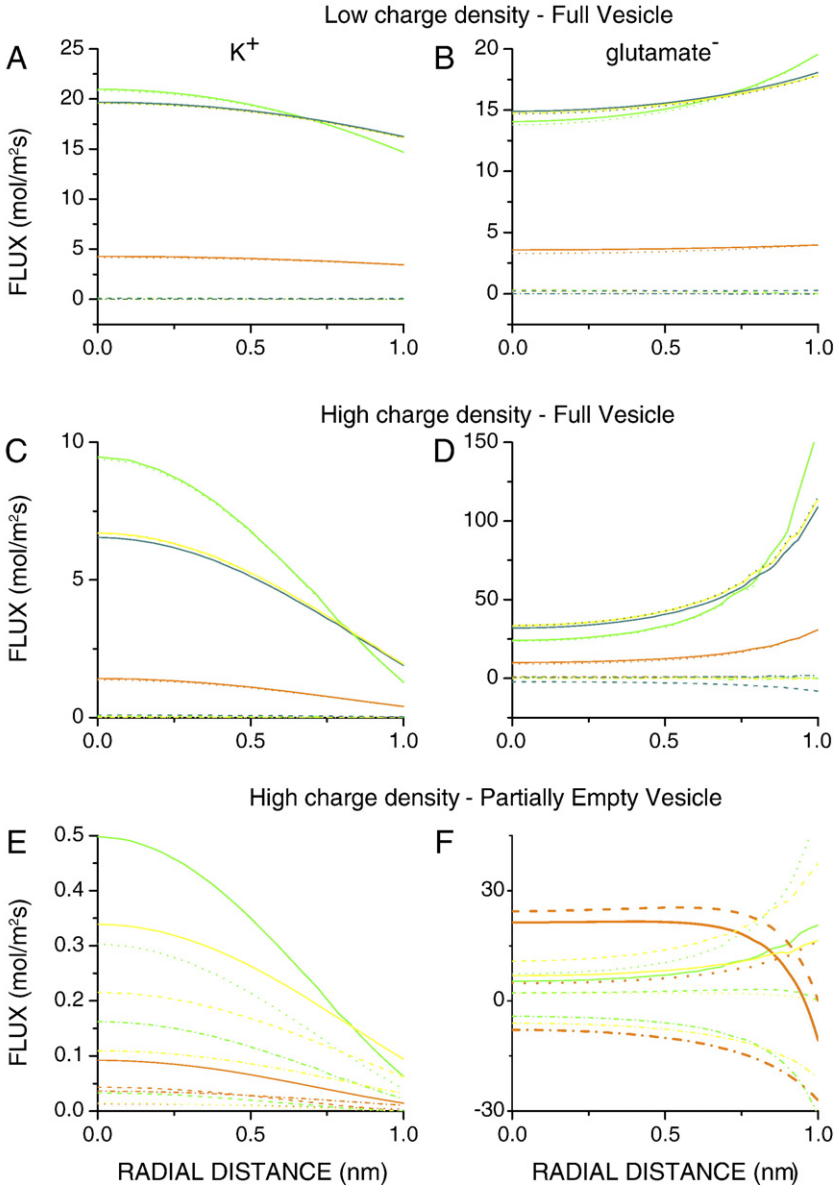


Fig. 7. Changing the permittivity and diffusion constants of ions and glutamate$^-$ in the nanopore had a significant effect on the radial profiles of $K^+$ and glutamate$^-$ fluxes, whereas the change of nanopore viscosity or fluid–wall boundary condition from non-slip to slip had only a marginal effect (see text). Green lines (nanopore permittivity—10); dark cyan (slip condition); yellow (nanopore fluid viscosity—2 mPas) and orange (diffusion constants of all ions and glutamate$^-$ in the nanopore was reduced by 80%). The pressure on the upper edge was $10^4$ Pa (dark cyan) or $10^5$ Pa (green, yellow and orange; B–C). The pore wall charge density was 8 mC/m$^2$ (dark cyan) or 64 mC/m$^2$ (green, yellow and orange), whereas the $K^+$–glutamate$^-$ concentration on the upper edge was 150 mM/l in all cases. $K^+$–glutamate$^-$ concentration on the controlling edges of the upper (vesicular) compartment was 150 mM/l ('Full Vesicle') or 15 mM/l ('Partially Empty Vesicle'). $K^+$–glutamate$^-$ concentration on the controlling edges of the lower (extra-cellular) compartment was 0 mM/l in all cases. $Na^+$–$Cl^-$ concentration was 0 mM/l (controlling edges of the upper compartment) and 150 mM/l (controlling edges of the lower compartment) in all cases.

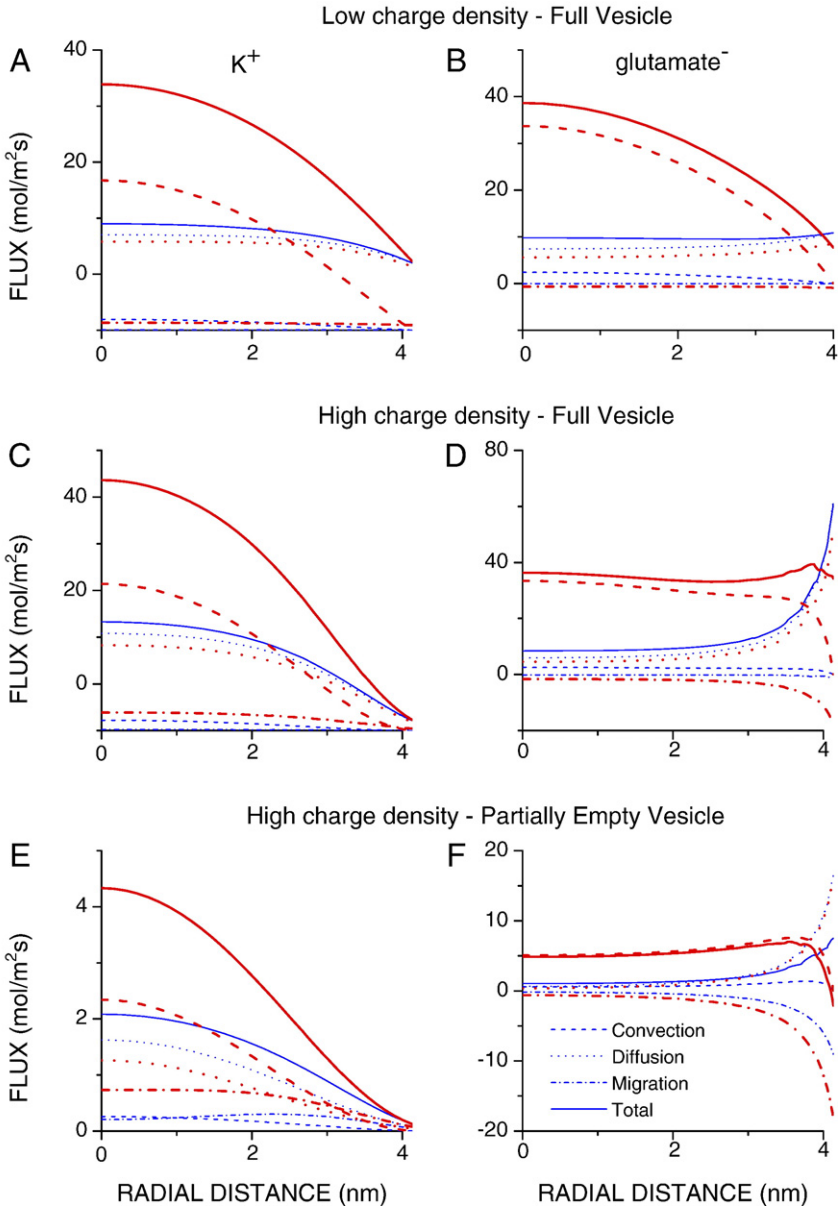


Fig. 8. Vesicular concentration of $K^+$–glutamate$^-$, pore charge density and external pressure gradient all affect the radial distribution of diffusive, migratory and convective fluxes in the middle of the wide pore (radius of 4 nm). The convective flux makes an important contribution, which becomes predominant when the external pressure gradient is high. The contribution of the migratory fluxes is also significant when the vesicle is partially empty. The fluxes usually diminish near the pore wall and the convective fluxes become zero (see text). The external pressure difference was $10^5$ Pa (blue lines) or $10^6$ Pa (red lines). The charge density on the pore wall was either 8 mC/m$^2$ ('low charge density') or 64 mC/m$^2$ ('high charge density'). $K^+$–glutamate$^-$ concentration on the controlling edges of the upper (vesicular) compartment was 150 mM/l ('Full Vesicle') or 15 mM/l ('Partially Empty Vesicle'). $K^+$–glutamate$^-$ concentration on the controlling edges of the lower (extra-cellular) compartment was 0 mM/l in all cases. $Na^+$–$Cl^-$ concentration was 0 mM/l (controlling edges of the upper compartment) and 150 mM/l (controlling edges of the lower compartment) in all cases.

Simulation of ion transport in ion channels is usually confined to the considerations of diffusion and drift, whilst the effect of water flux on ion transport is ignored [26,27,30,42]. Description of the transport of transmitter or ions through the fusion pore however, cannot ignore the effect of water flux given the intra-vesicular pressure, which appears to be quite significant [22,23]. The coupled system of Poisson–Nernst–Planck and Navier–Stokes equations was therefore used to calculate the concentration and fluxes (diffusive, migratory and convective) of $K^+$ and glutamate$^-$, fluid (water) velocity and pressure through a computational domain consisting of a charged nanofluidic pore 10 nm long and whose radius ranged from 1 nm ('narrow' pore) to 4 nm ('wide' pore), or in some cases to 8 nm. The pore was flanked on each side with a compartment representing the vesicular interior and extracellular space [26–32]. Briefly the simulation conditions were as follows (for details see Methods and Results). The surface charge was positive and its density on the membrane facing the pore ranged from $8\times10^{-3}$ to $64\times10^{-3}$ C/m$^2$, but the density was zero on the membrane facing two compartments. There was no potential difference between the control boundaries of the upper (vesicular) and lower (extracellular) compartments. The

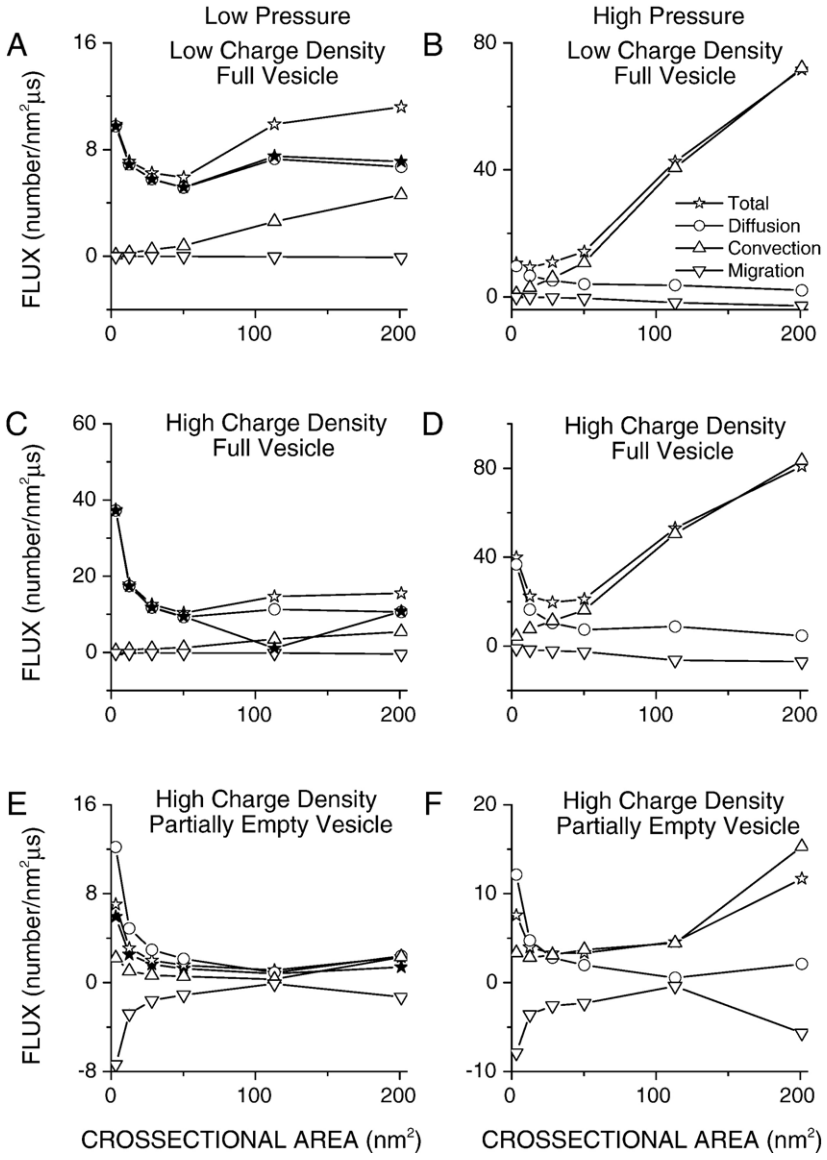


Fig. 9. Mean unitary diffusive, migratory, convective and total fluxes of glutamate$^-$ with low ($10^5$ Pa; A, C and E) or high ($10^6$ Pa; B, D and F) external pressure gradient (see text). With low external pressure gradient the diffusive flux dominates, but when the vesicle is partially empty and pore widens the convective flux makes an important contribution. Note that the mean unitary diffusive flux tends to diminish as the pore widens, but also that the convective flux completely dominates when pore widens if the pressure gradient is high. The charge density on the pore wall was either 8 mC/m$^2$ ('low charge density') or 64 mC/m$^2$ ('high charge density'). $K^+$–glutamate$^-$ concentration on the controlling edges of the upper (vesicular) compartment was 150 ('Full Vesicle') or 15 mM/l ('Partially Empty Vesicle'). Note that No-NS (filled stars; A, C and E) gives mean unitary total fluxes calculated without Navier–Stokes equation (see text). In all cases $K^+$–glutamate$^-$ concentration on the controlling edges of the lower (extra-cellular) compartment was 0 mM/l, whilst $Na^+$–$Cl^-$ concentration was 0 mM/l (upper compartment) or 150 mM/l (lower compartment).

pressure difference between two control boundaries (on the upper and lower compartment) ranged from $10^4$ to $10^6$ Pa. The $K^+$–glutamate$^-$ concentration in the upper compartment ranged from 5 mM/l to 150 mM/l, and was 0 mM/l in the lower compartment. $Na^+$–$Cl^-$ concentration was 0 mM/l in the upper compartment and 150 mM/l in the lower compartment. The following are most important conclusions of this study.

### *4.2. Pressure and fluid velocity*

Pressure in a nano-fluidic system can arise from two sources: a) the external pressure on the controlling edges of the 'vesicular' and 'extra-cellular' compartments flanking the nanopore, and) the pressure induced by the electrokinetic force arising from the presence of mobile ions in the pore and fixed charges on the pore wall. Both contributions are important and both are largely confined to the nanopore interior. The induced pressure (which is negative) can significantly surpass the external pressure difference, even when the external pressure difference approaches its maximal physiological value of $1.2\times10^6$ Pa [22,23]. The induced pressure is large near the pore wall, which renders the total pressure in the pore radially non-uniform (in the absence of fixed charges on the pore wall the pressure is radially uniform). The contribution of the

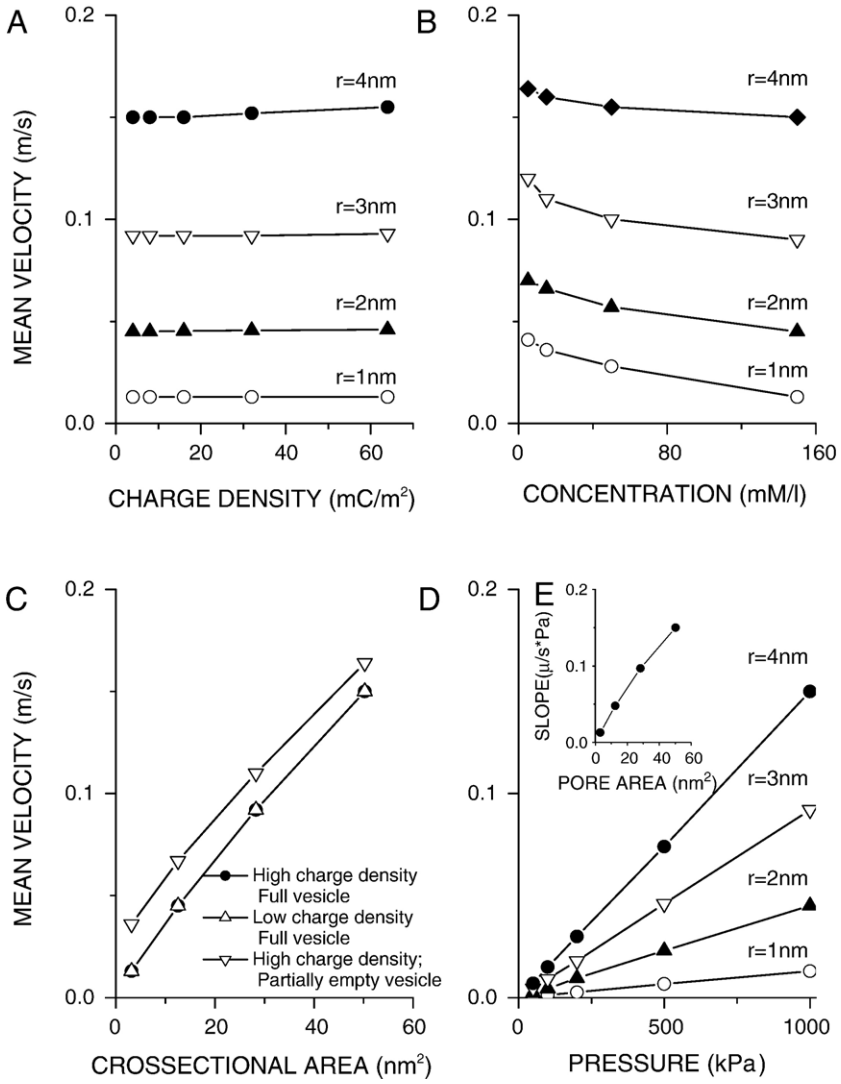


Fig. 10. (A) Mean fluid velocity rises only marginally as the pore wall charge density increases irrespective of pore radius. (B) Mean fluid velocity is higher when the vesicle is Partially empty. (C) Mean fluid velocity rises, but sub-linearly as the pore cross-sectional area widens. (D) Mean fluid velocity vs. external pressure relationship is linear. (E) The slope of the mean fluid velocity vs. external pressure relationship increases almost linearly with the pore cross-sectional area.

induced pressure is significant even in the center of the narrow pore, but not of the wide pore. Finally the negative pressure in the fusion pore is also of interest as it demonstrates the existence of force, which would tend to close the fusion pore, although it is still to be determined whether the force is large enough to cause a pore closure. Raising the membrane permittivity (from 2 to 10), or the fluid viscosity (from 1 to 2 mPa) or lowering the diffusion constant of ions and glutamate$^-$ in the nanopore by 80% alters the pressure only marginally. However, lowering the permittivity in the nanopore makes the pressure less negative in the pore center but more negative near the pore wall.

The fluid (water) velocity field consists also of two parts—flow velocity driven by the external pressure (Poiseuille flow) and electro-osmotic flow velocity. Although the efflux of water is a consequence of the pressure gradient (external and induced) the spatial profiles of pressure and fluid velocity differ greatly. The fluid velocity, which is the highest in the pore center, diminishes to zero near the pore wall (no-slip condition). The frictional force, which is proportional to the radial gradient of the fluid velocity (and which is the greatest near the pore wall), provides a partial compensatory mechanism to the pressure gradient that drives the fluid flow. The osmotic force, which is proportional to the concentration gradient of ions and glutamate$^-$, could provide an additional compensatory mechanism opposing the fluid flow and contributing to the mismatch between pressure and velocity spatial profiles.

Along the pore axis the fluid velocity is constant. It tapers-off quickly away from the pore, and the rate of tapering is faster if the pore is narrow. Whereas the changes of the permittivity (in the nanopore or in the membrane) or those of the diffusion constant of ions (or glutamate$^-$) in the nanopore have only a marginal effect on the fluid velocity, lowering the fluid viscosity not unexpectedly reduced the fluid velocity. The fluid velocity is changed the most if a slip (instead of non-slip) boundary condition is assumed at the fluid–membrane interface. The velocity is not only much greater, but its radial profile in the

nanopore is flat instead of diminishing to zero near the pore wall. This is of general interest for understanding of the permeation of water through ion channels and pores with hydrophobic lining such as mechanosensitive channels, or of hydrophobic carbon nanotubes.

The relationships of fluid velocity to external pressure gradient, or to pore radius and vesicular concentration of $K^+$–glutamate$^-$ were examined in detail. The fluid velocity averaged over the cross-sectional area in the pore center (mean fluid velocity) rises as the pore widens, and the relationship is very pronounced—not proportional to the pore radius, but to the pore cross-sectional area. Mean fluid velocity increases linearly with pressure gradient, and the slope of their relationship is also almost linearly related to the cross-sectional pore area. As the pore widens the fluid velocity thus becomes not only larger, but also more sensitive to the changes of external pressure gradient. Mean velocity does not depend strongly on the pore charge density. This may appear puzzling given that the induced pressure is substantial. However, two factors limit the importance of the induced pressure on the mean fluid velocity. As already discussed there is a spatial mismatch between the induced pressure and the fluid velocity. Whilst near the pore wall the induced pressure is the highest the fluid velocity is very low owing to the no-slip constraints. In addition, although the magnitude of the induced pressure along the axis of the pore first increases, it subsequently decreases reaching the value near that on the controlling edge of the compartment flanking the exit. Nevertheless note that the fluid velocity rises as the vesicular concentration of $K^+$–glutamate$^-$ diminishes, and the effect is relatively more important for narrow pores. The physiological importance is that the water efflux will increase as the vesicle empties its glutamate content. We did not explore what caused such an effect, but as the $K^+$–glutamate$^-$ concentration diminishes the nanopore becomes electrostatically more compact, its radial profiles of $K^+$ and glutamate$^-$ concentration (and fluxes) more uniform, i.e. more prominent in the pore center, and thus more able to contribute to the kinetically driven flow of fluid.

### 4.3. Spatial distribution of glutamate$^-$ and $K^+$ concentration is largely determined by fusion pore charge density

As expected the concentration of $K^+$ (co-ion) is suppressed, and of glutamate$^-$ (counter-ion) enhanced in the positively charged pore [26,27,32]. The effect is greater the higher the charge density, and narrower the pore. It is also more pronounced near the pore wall. This renders the distribution of $K^+$, but even more of glutamate$^-$, much more non-uniform radially in the wide pore. Even when it reaches physiologically maximal levels, the external pressure gradient has a very modest effect, and alters the $K^+$ and glutamate$^-$ concentration in the pore interior only modestly, and only if the pore is wide.

Since protein domains of charged and hydrophilic side-chains, but also the lipid headgroup region, immediately contacting the ions in the fusion pore, are highly polar, we evaluated whether significantly greater permittivity (10 instead of 2) of the membrane would alter the $K^+$ or glutamate$^-$ profiles in the nanopore, but this was not the case. Greater fluid viscosity (2 instead of 1 mPas) or lower diffusion constant of ions and glutamate (lower by 80%) made also very little difference. Lowering the diffusion to one fifth of its value is considered as appropriate since earlier molecular dynamics simulations have shown that the diffusion constant can be much lower in the confined space of an ion channel [45]. In contrast reducing the permittivity in the nanopore to half its value did alter the concentration profiles of both $K^+$ and glutamate$^-$.

In the present study we focused on the transport of glutamate$^-$ through a positively charged nanopore. However, this study also casts a light on the transport of other transmitters such as acetylcholine and norepinephrine, which are positively charged at neutral pH, and with the fusion pore either positively or negatively charged. The diffusion constants of acetylcholine and norepinephrine ($0.40\times10^{-9}$ m$^2$/s and $0.60\times10^{-9}$ m$^2$/s respectively) [46–48] are similar to the diffusion constant of glutamate$^-$, and are not very different from the diffusion constants of $K^+$, $Na^+$ and $Cl^-$ (see Methods). If the charge of the transmitter differs from the charge on the wall of the nanopore (i.e. if it can be considered as a counter-ion) it will behave as the glutamate$^-$ in the present study, but if its charge is the same (i.e. if it can be considered as a co-ion) its transport will be similar to the transport of $K^+$.

### 4.4. Diffusional, migratory and convective fluxes

Diffusional, migratory and convective fluxes all make a contribution to the total flux of $K^+$ and glutamate$^-$. The diffusive $K^+$ flux clearly dominates, except when the vesicle is partially empty, when the convective and migratory $K^+$ fluxes make a small contribution. The spatial distribution of the diffusive $K^+$ flux and $K^+$ concentration are similar (they are highest in the middle of the pore), and are controlled by the pore wall charge density (the diffusion flux vs. charge density relationship is inverse). The convective $K^+$ flux also decreases near the pore wall, becoming zero at the wall surface (a consequence of no-slip condition). The glutamate$^-$ fluxes are also largely diffusive, and are generally greater than $K^+$ fluxes (glutamate$^-$ is a ‘counter-ion’ and its concentration in the pore is higher), and moreover rise near the pore wall, and the rise depends on the charge density on the pore wall. The convective glutamate$^-$ flux becomes important when the intra-vesicular pressure is high, and becomes dominant if the pore is also wide. The vesicular pressure can thus be an important factor in flushing-out the glutamate in the later stages of release of vesicular content [19]. Membrane permittivity and nanopore viscosity do not affect either $K^+$ or glutamate$^-$ fluxes. The effect of the fluid–wall interface boundary condition was evaluated only at low external pressure gradients ($10^4$ Pa), and also appeared to have only a marginal effect. In contrast, but not unexpectedly, lower diffusion constant of ions and glutamate$^-$ led to lower fluxes. Finally, lower permittivity in the nanopore led to higher $K^+$ fluxes in the pore center but lower near the wall. Opposite was the case for glutamate$^-$ fluxes.

In order to compare the ability of fusion pores of different geometries to transport the glutamate$^-$ we calculated the unitary mean fluxes of glutamate$^-$(mean fluxes per unit cross-sectional area of the pore). At low external pressure gradient ($10^5$ Pa or approximately one tenth of the maximal physiological intra-vesicular pressure gradient) the contribution of the convective glutamate$^-$ flux is generally small except when pore becomes very wide (i.e. when its radius is 6–8 nm) and the simulations that completely ignored the interactions of glutamate$^-$, $K^+$, $Na^+$ and $Cl^-$ with water gave very similar values. If the external pressure is high ($10^6$ Pa, i.e. close to the maximal physiological pressure) the convective glutamate$^-$ flux makes an important contribution to the total flux, becoming dominant as the pore widens. The unitary mean convective flux however is much reduced if the vesicular $K^+$–glutamate$^-$ concentration decreases (partially empty vesicle), and becomes essentially independent of the pore radius. Interestingly the unitary mean diffusive glutamate$^-$ flux is lower for wide pores irrespective of external pressure, especially when the charge density is high. An approximate neutrality of the charges in the nanopore and on the pore wall, leads to the greater glutamate$^-$ concentration (counter-ion), and thus to higher glutamate$^-$ fluxes in narrow nanopores. Although a similar degree of electrical neutrality is maintained in both cases the ratio of nanopore volume and its surface wall area is lower for narrow nanopores. If the external pressure is low the unitary mean total glutamate$^-$ flux diminishes as the pore widens (diffusive glutamate$^-$ flux dominates), but rises if the external pressure is high, due to the greater contribution of convective flux.

Word of caution is necessary however. The permittivity and diffusion constant of ions and glutamate$^-$ might not be just lower (and fluid viscosity higher) due to the confinement in the nanopore than in the bulk, but it might also be inhomogeneous owing to the interactions with the pore wall and with water molecules. Water concentration is also known to be highly non-uniform in the nanopores [31]. Such 'deviations' from the assumptions of continuum theory can lead to errors in the estimations of pressure, fluid velocity, ion and glutamate$^-$ concentration and flux.

## 5. Conclusion

In conclusion we provide a general treatment of combined diffusion/migration/fluid flow through charged nano-pores, using continuum theory. The study demonstrates that the intra-vesicular pressure can be an important factor in 'flushing-out' the transmitter, and its importance rises during the late stage of exocytosis when the pore widens. The intra-vesicular pressure, but also the pressure induced by the movement of mobile charged particles such as glutamate$^-$, $K^+$, $Na^+$ and $Cl^-$, whose concentration and spatial distribution are determined by the charge density on the pore wall (electro-kinetically induced pressure) control the efflux of water. Surprisingly, as the vesicle empties its transmitter content the electro-kinetically driven flow increases, and the water is 'dragged-out' into the extracellular space more efficiently.

## Acknowledgments

Supported by the grants from the National Science and Engineering Council of Canada and Canadian Institutes of Health Research to M.I.G.

## References

[1] S. Redman, Quantal analysis of synaptic potentials in neurons of the central nervous system, Physiol. Rev. 70 (1990) 165–198.
[2] T.J. Schroeder, J.A. Jankowski, J. Senyshyn, R.W. Holz, R.M. Wightman, Zones of exocytotic release on bovine adrenal medullary cells in culture, J. Biol. Chem. 269 (1994) 17215–17220.
[3] A. Walker, M.I. Glavinović, J.M. Trifaro, Temperature dependence of release of vesicular content in bovine chromaffin cells, Pflugers Arch. - Eur. J. Physiol. 432 (1996) 885–892.
[4] S. Sulzer, E.N. Pothos, Regulation of quantal size by presynaptic mechanisms, Rev. Neurosci. 11 (2000) 159–212.
[5] V.A. Klyachko, M.B. Jackson, Capacitance steps and fusion pores of small and large-dense-core vesicles in nerve terminals, Nature 418 (2002) 89–92.
[6] S. Kebir, F. Aristizabal, D. Maysinger, M.I. Glavinović, Rapid change of quantal size in PC-12 cells detected by neural networks, J. Neurosci. Methods 142 (2005) 231–242.
[7] L.M. Wahl, C. Pouzat, K.J. Stratford, Monte Carlo simulation of fast excitatory synaptic transmission at a hippocampal synapse, J. Neurophysiol. 75 (1996) 597–608.
[8] M.I. Glavinović, Monte Carlo simulation of vesicular release, spatio-temporal distribution of glutamate in synaptic cleft, and generation of postsynaptic currents, Pflugers Arch. 437 (1999) 462–470.
[9] Y. Levin, M.A. Idiart, J.J. Arenzon, Random walk to freedom: the time of effusion, Physica, A Stat. Mech. Appl. 354 (2005) 95–100.
[10] J.M. Fernandez, M. Villalon, P. Verdugo, Reversible condensation of mast cell secretory products in vitro, Biophys. J. 59 (1991) 1022–1027.
[11] M.J. Curran, M.S. Brodwick, Ionic control of the size of the vesicle matrix of beige mouse mast cells, J. Gen. Physiol. 98 (1991) 771–790.
[12] J.R. Monck, A.F. Oberhauser, G. Alvarez de Toledo, J.M. Fernandez, Is swelling of the secretory granule matrix the force that dilates the exocytotic fusion pore? Biophys. J. 59 (1991) 39–47.
[13] L.J. Breckenridge, W. Almers, Currents through the fusion pore that forms during exocytosis of a secretory vesicle, Nature 328 (1987) 814–817.
[14] J. Zimmerberg, M. Curran, F.S. Cohen, M. Brodwick, Simultenous electrical and optical measurements show that membrane fusion precedes secretory granule swelling during exocytosis of beige mouse mast cells, Proc. Natl. Acad. Sci. U. S. A. 84 (1987) 1585–1589.
[15] S. Terakawa, J.H. Fan, K. Kumakura, M. Ohara-Imaizumi, Quantitative analysis of exocytosis directly visualized in living chromaffin cells, Neurosci. Lett. 123 (1991) 82–86.
[16] S. Terakawa, S. Manivannan, K. Kumakura, Evidence against the swelling hypothesis for initiation of exocytosis in terminals of chromaffin cell processes, J. Physiol.(Paris) 87 (1993) 209–213.
[17] A. Finkelstein, J. Zimmerberg, F.S. Cohen, Osmotic swelling of vesicles: its role in the fusion of vesicles with planar phospholipid bilayer membranes and its possible role in exocytosis, Annu. Rev. Physiol. 48 (1986) 163–174.
[18] R.W. Holz, The role of osmotic forces in exocytosis from adrenal chromaffin cells, Annu. Rev. Physiol. 48 (1986) 175–189.
[19] T. Tsuboi, T. Kikuta, T. Sakurai, S. Terakawa, Water secretion associated with exocytosis in endocrine cells revealed by micro forcemetry and evanescent microscopy, Biophys. J. 83 (2002) 172–183.
[20] ML. Kelly, W.J. Cho, A. Jeremic, R. Abu-Hamdah, P.B. Jena, Vesicle swelling regulates content expulsion during secretion, Cell Biol. Int. 28 (2004) 709–716.
[21] P.B. Jena, Cell secretion and membrane fusion, J. Endocrinol. 5 (2005) 1–20.

[22] C. Nanavati, J.M. Fernandez, The secretory granule matrix: a fast-acting smart polymer, Science 259 (1993) 963–965.
[23] P.E. Marszalek, A.F. Oberhauser, H. Li, J.M. Fernandez, The Force-driven conformations of heparin studied with single molecule force microscopy, Biophys. J. 85 (2003) 2696–2704.
[24] A. Jeremic, W.J. Cho, B.P. Jena, Involvement of water channels in synaptic vesicle swelling, Exp. Biol. Med. 230 (2005) 674–680.
[25] G. Soveral, R.I. Macey, T.F. Moura, Membrane stress causes inhibition of water channels in brush border membrane vesicles from kidney proximal tubule, Biol. Cell 89 (1997) 275–282.
[26] W. Nonner, L. Catacuzzeno, B. Eisenberg, Binding and selectivity in L-type calcium channels: a mean spherical approximation, Biophys. J. 79 (2000) 1976–1992.
[27] B. Corry, S. Kuyucak, S.H. Chung, Tests of continuum theories as models of ion channels. II. Poisson Nernst Planck theory versus brownian dynamics, Biophys. J. 78 (2000) 2364–2381.
[28] B. Corry, S. Kuyucak, S.H. Chung, Dielectric self-energy in Poisson–Boltzmann and Poisson Nernst Planck models of ion channels, Biophys. J. 84 (2003) 3594–3606.
[29] N.A. Patankar, H.H. Hu, Numerical simulation of electroosmotic flow, Anal. Chem. 70 (1998) 1870–1881.
[30] W. Nonner, B. Eisenberg, Ion permeation and glutamate residues linked by Poisson–Nernst–Planck theory in L-type calcium channels, Biophys. J. 75 (1998) 1287–1305.
[31] R. Qiao, N.R. Aluru, Ion concentrations and velocity profiles in nanochannel osmotic flows, J. Chem. Phys. 118 (2003) 4692–4701.
[32] H. Daiguji, P. Yang, A. Majumdar, Ion transport in nanofluidic channels, Nano Lett. 4 (2004) 137–142.
[33] S.G.A. McLaughlin, G. Szabo, G. Eisenman, Divalent ions and the surface potential of charged phospholipid membranes, J. Gen. Physiol. 58 (1971) 667–687.
[34] B. Hille, A.M. Woodhull, B.I. Shapiro, Negative surface charge near sodium channels of nerve: divalent ions, monovalent ions, and pH, Philos. Trans. R. Soc. Lond., B Biol. Sci. 270 (1975) 301–318.
[35] J. Barthel, H. Krienke, W. Kunz, Physical Chemistry of Electrolyte Solutions: Modern Aspects, Springer, New York, 1998.
[36] S. Durand-Vidal, J.-P. Simonin, P. Turq, Electrolytes at Interfaces, Kluwer, Boston, 2000.
[37] S.W. Chiu, J.A. Novotny, E. Jakobsson, The nature of ion and water barrier crossings in a simulated ion channel, Biophys. J. 64 (1993) 96–108.
[38] R. Qiao, N.R. Aluru, Atypical dependence of electroosmotic transport on surface charge in a single-wall carbon nanotube, Nano Lett. 3 (2003) 1013–1017.
[39] B.P. Jena, S.J. Cho, A. Jeremic, M.H. Stromer, R. Abu-Hamdah, Structure and composition of the fusion pore, Biophys. J. 84 (2003) 1337–1343.
[40] X. Han, M.B. Jackson, Structural transitions in the synaptic SNARE complex during Ca2+-triggered exocytosis, J. Cell Biol. 172 (2006) 281–293.
[41] P.R. Maycox, T. Deckwerth, J.W. Hell, R. Jahn, Glutamate uptake by brain synaptic vesicles. Energy dependence of transport and functional reconstitution in proteoliposomes, J. Biol. Chem. 263 (1988) 15423–15428.
[42] G. Moy, B. Corry, S. Kuyucak, S.H. Chung, Tests of continuum theories as models of ion channels. I. Poisson–Boltzmann theory versus Brownian dynamics, Biophys. J. 78 (2000) 2349–2363.
[43] J.O.M. Bockris, A.K.N. Reddy, Modern Electrochemistry, Plenum Publ., New York, 1976.
[44] J.S. Newman, Electrochemical Systems, 2nd ed.Prentice Hall, Englewood Cliffs, NJ, 1991.
[45] G.R. Smith, M.S.P. Sansom, Effective diffusion coefficients of $K^+$ and $Cl^-$ ions in ion channel models, Biophys. Chem. 79 (1999) 129–151.
[46] A. Walker, M.I. Glavinović, J.M. Trifaro, Time course of release of content of single vesicles in bovine chromaffin cells, Pflügers Arch. 431 (1996) 729–735.
[47] K. Tai, S.D. Bond, H.R. MacMillan, N.A. Baker, M.J. Holst, J.A. McCammon, Finite element simulations of acetylcholine diffusion in neuromuscular junctions, Biophys. J. 84 (2003) 2234–2241.
[48] M.R. Bennett, L. Farnell, W.G. Gibson, D. Blair, A quantitative description of the diffusion of noradrenaline in the media of blood vessels following its release from sympathetic varicosities, J. Theor. Biol. 226 (2004) 359–372.